

Article

A Process-Oriented Approach to Identify Evolutions of Sea Surface Temperature Anomalies with a Time-Series of a Raster Dataset

Lianwei Li ¹, Yangfeng Xu ^{1,2}, Cunjin Xue ^{2,3,*} , Yuxuan Fu ^{1,2} and Yuanyu Zhang ^{1,2}

¹ College of Oceanography and Space Informatics, China University of Petroleum, Qingdao 266580, China; 20050046@upc.edu.cn (L.L.); z19160008@s.upc.edu.cn (Y.X.); z20160120@s.upc.edu.cn (Y.F.); z20160119@s.upc.edu.cn (Y.Z.)

² Key Laboratory of Digital Earth Science, Chinese Academy of Sciences, Beijing 100094, China

³ Aerospace Information Research Institute, Chinese Academy of Sciences, Beijing 100094, China

* Correspondence: xuecj@aircas.ac.cn; Tel.: +86-10-82178126

Abstract: It is important to consider where, when, and how the evolution of sea surface temperature anomalies (SSTA) plays significant roles in regional or global climate changes. In the comparison of where and when, there is a great challenge in clearly describing how SSTA evolves in space and time. In light of the evolution from generation, through development, and to the dissipation of SSTA, this paper proposes a novel approach to identifying an evolution of SSTA in space and time from a time-series of a raster dataset. This method, called PoAIES, includes three key steps. Firstly, a cluster-based method is enhanced to explore spatiotemporal clusters of SSTA, and each cluster of SSTA at a time snapshot is taken as a snapshot object of SSTA. Secondly, the spatiotemporal topologies of snapshot objects of SSTA at successive time snapshots are used to link snapshot objects of SSTA into an evolution object of SSTA, which is called a process object. Here, a linking threshold is automatically determined according to the overlapped areas of the snapshot objects, and only those snapshot objects that meet the specified linking threshold are linked together into a process object. Thirdly, we use a graph-based model to represent a process object of SSTA. A node represents a snapshot object of SSTA, and an edge represents an evolution between two snapshot objects. Using a number of child nodes from an edge's parent node and a number of parent nodes from the edge's child node, a type of edge (an evolution relationship) is identified, which shows its development, splitting, merging, or splitting/merging. Finally, an experiment on a simulated dataset is used to demonstrate the effectiveness and the advantages of PoAIES, and a real dataset of satellite-SSTA is used to verify the rationality of PoAIES with the help of ENSO's relevant knowledge, which may provide new references for global change research.



Citation: Li, L.; Xu, Y.; Xue, C.; Fu, Y.; Zhang, Y. A Process-Oriented Approach to Identify Evolutions of Sea Surface Temperature Anomalies with a Time-Series of a Raster Dataset. *ISPRS Int. J. Geo-Inf.* **2021**, *10*, 500. <https://doi.org/10.3390/ijgi10080500>

Academic Editor: Wolfgang Kainz

Received: 6 May 2021

Accepted: 20 July 2021

Published: 23 July 2021

Publisher's Note: MDPI stays neutral with regard to jurisdictional claims in published maps and institutional affiliations.



Copyright: © 2021 by the authors. Licensee MDPI, Basel, Switzerland. This article is an open access article distributed under the terms and conditions of the Creative Commons Attribution (CC BY) license (<https://creativecommons.org/licenses/by/4.0/>).

1. Introduction

Sea surface temperature (SST) is an essential marine variable [1] and plays an important role in climate change monitoring, weather forecasting, and marine fishery monitoring [2,3]. Sea surface temperature anomaly (SSTA) variations refer to the abnormal increase or decrease in SST over a specified spatial domain and for a specified time [4], and SSTA variations have a property of evolution from generation to development and dissipation in space and time. The evolution of SSTA in a specified space and time may be a driver or a responder to extreme regional climate events such as El Niño-Southern Oscillation (ENSO) [5]. ENSO is an interannual phenomenon that promotes change in the surface winds and, consequently, in the SST distribution of the Pacific Ocean [6]. El Niño and La Niña are the warm and cold SSTA phases of ENSO phenomena.

The Multivariate ENSO Index (MEI) is often used to identify ENSO events, which is divided into eastern Pacific ENSO (EP ENSO) and central Pacific ENSO (CP ENSO) based on different spatial distributions of the maximum SSTA [7–9]. The transformation of variations of SSTA from the Eastern Pacific Ocean to Central Pacific Ocean can be used to define a new ENSO index and to identify ENSO events [10], and SSTA has a certain and concretely assessable impact on ENSO events in the North and South Pacific Ocean [11]. Additionally, Xue et al. and Liu et al. found that the splitting or merging of SSTA between successive time snapshots would strengthen or weaken an ENSO's intensity [12,13]. Thus, it is important to know where, when, and how the SSTA variation and evolution play a significant role in regional or global climate changes. Additionally, the advanced earth-observing technologies, combined with historical climate records, make it possible to acquire and analyze the dynamic information of SSTA on a large scale [14].

With a time-series of a raster dataset, there has been considerable literature around addressing dynamic characteristics of SST, and among them, cluster-based mining methods were widely used to analyze variations of SSTA [15]. A cluster-based method takes similar variations of SSTA within a spatiotemporal domain as one cluster, e.g., Steinbach et al. used the K-Mean and the Density-Based Spatial Clustering of Applications with Noise (DBSCAN) to explore the time-averaged spatial distribution of SSTA [16]; Birant and Kut developed the ST-DBSCAN algorithm to explore spatiotemporal clustering patterns of marine parameters [17]; Kawale et al. took a time as an additional dimension and designed a method based on shared reciprocal nearest neighbors to find the global dipole modes of SSTA [18]; and Xue et al. proposed a kernel expansion algorithm to discover a spatial sensitive region and its temporal duration of SSTA [19]. While these studies obtained good results on the instantaneous states of SSTA at the time snapshots—which we call snapshot objects of SSTA, as there are few considerations related to the evolution relationships of SSTA from the last through to the current and next snapshot [20]—there is a lack of dynamic information of SSTA within successive time snapshots.

To deal with geographical dynamics, a large number of models were proposed to describe the evolution relationships among geographical entities [21,22]. To clearly address geographical entities and their evolutions and interactions, a graph-based spatiotemporal, representing, and identifying model was proposed [23,24]. Four kinds of relationships, i.e., an initiation, a development, a movement, and a cessation, were defined, and an area-overlapping-based method was used to identify these relationships from rainstorms [25]. Additionally, an instance of an urban heat island (UHI) zone was taken as a node, an evolving relationship between two UHI zones at successive time snapshots as an edge, and an overlapped area threshold was used to identify six kinds of evolving relationships, i.e., an appearance/disappearance, an expansion, a contraction, a continuation, a merging, and a splitting between two nodes [26]. While these definitions and identifications play a foundational role in mining evolutions of SSTA, the method based on spatiotemporal topologies of snapshot objects is based on the precondition that the geographical entities at instant time snapshots are independent. In this way, the evolution relationship of SSTA between successive time snapshots is isolated. In addition, the overlapping techniques have difficulties in dealing with geographic entities in fast-moving speed cases, as it is likely that no overlapping at all will occur [27,28], and the linking threshold of tracking successive snapshot objects is subjective. To describe evolutions and temporal behaviors between successive image objects, Guttler et al. designed a set of evolution graphs to extract and characterize spatiotemporal dynamics [29]. Xue et al. also improved a graph-based representing model and defined six kinds of relationships, i.e., a generation, a development, a merging, a splitting, a merging/splitting, and a termination to analyze SSTA evolutions [12]. However, these methods provide no strategy to identify evolutions among successive time snapshots.

To overcome the above deficiencies, Xue et al. took a process evolution from generation to development and dissipation as a representative and analyzed the scale to deal with SSTA variations [12,30,31]. The evolution process ensured the continuity of SSTA in

space and time. Additionally, by taking a process-oriented idea, Liu et al. proposed the Dual-constraint Spatiotemporal Clustering Approach (DcSTCA) to discover the clustering patterns of marine anomaly variations [20]. As a comprehensive consideration of spatial, temporal, and thematic characteristics of marine parameters, the DcSTCA obtained continuous SSTA in space and time. However, DcSTCA focuses on an issue with the snapshot objects of SSTA belonging to the same spatiotemporal cluster and does not consider how a snapshot object evolves from the previous through to the current and next snapshot, which limits its capability to analyze geographical dynamics.

To overcome the above shortcomings and to improve the geographic dynamic analysis capabilities of SSTA spatiotemporal clusters, this work took full consideration of the evolutions of SSTA in space and time in order to design a process-oriented approach to obtain process objects of SSTA with a time-series of a raster dataset. The process objects of SSTA include snapshot objects of SSTA and their evolution relationships. Our proposed method, which we named the Process-oriented Approach for Identifying Evolutions of SSTA (PoAIES), is a method based on DcSTCA for extracting the inherent evolutionary relationships of spatiotemporal clusters. The rest of this paper is organized as follows. Section 2 designs a workflow of PoAIES in view of the evolution process and describes its key steps in detail. In Section 3, a simulated dataset and a time-series from a global SST remote-sensing dataset are used to evaluate the PoAIES. Section 4 summarizes and discusses our conclusions.

2. PoAIES Algorithm

This paper called an evolution object of SSTA from generation to development and dissipation as a process object. A process object of SSTA includes spatial snapshot objects and their evolution relationships between snapshots. The evolution relationship is one of four types, i.e., a development, a merging, a splitting, and a splitting/merging relationship [12], and the role played by evolution relationships is called evolution characteristics, which are more obvious in terms of splitting and merging. Generally, when SSTA are merging, the intensity of the snapshot object at the next moment will be stronger, and the intensity of the snapshot object at the next moment will be weaker when the SSTA is splitting.

- **A development relationship:** Representing no interaction with other objects as one object moves from the previous to the current and then to the next snapshot.
- **A merging relationship:** Representing an interaction where two or more snapshot objects in the previous time snapshot merge into one object in the current time snapshot.
- **A splitting relationship:** Representing an interaction where one snapshot object in the current time snapshot split into two or more snapshot objects in the next time snapshot.
- **A splitting/merging relationship:** Representing an interaction where a part of one snapshot object and a part or whole of another snapshot object in the previous time snapshot merge into a new snapshot object in the current time snapshot.

Thus, in order to convert a time-series of a raster dataset into the process objects of SSTA, PoAIES needs to deal with four key steps: (1) extracting spatial snapshot objects of SSTA from a time-series of raster dataset; (2) constructing spatial snapshot objects of SSTA into process objects; (3) graph-based representation on process objects of SSTA; and (4) identifying evolution relationships of SSTA from graph-based process objects. Figure 1 shows a workflow of PoAIES.

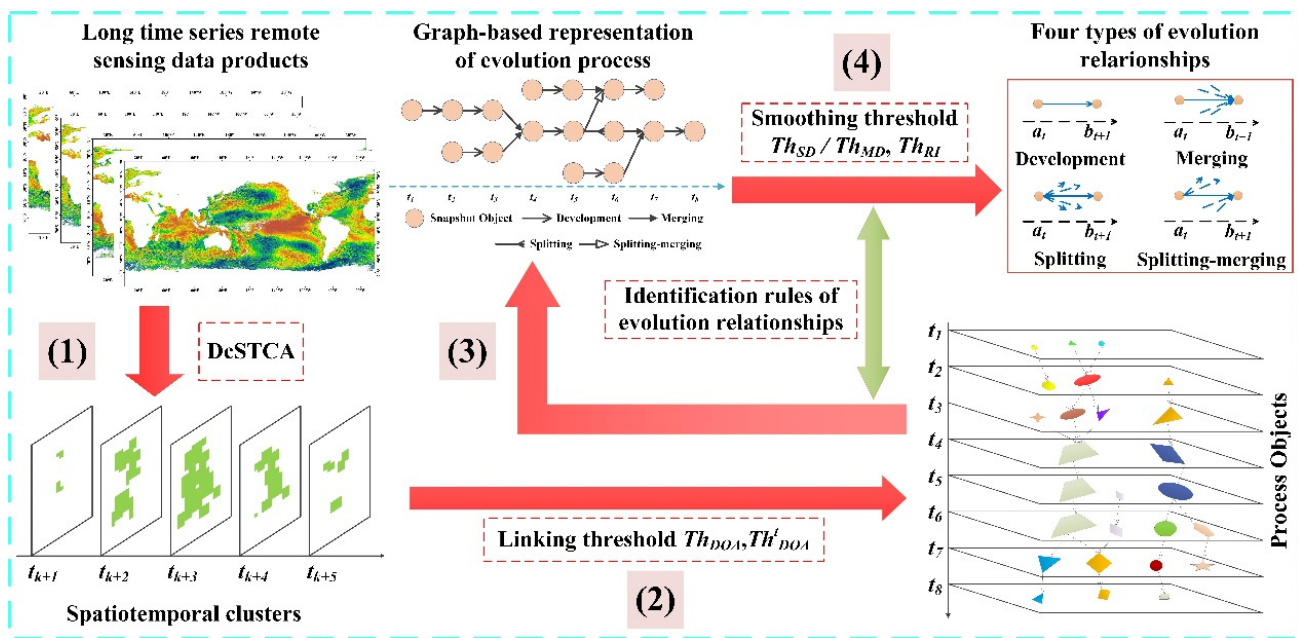


Figure 1. A workflow of PoAIES. (1)–(4) represent the four key steps of the PoAIES. The red arrow represents a processing step, the dashed box represents a method or a condition used in each step, and the green double-headed arrow represents a method or a condition used in different steps.

2.1. Extracting Snapshot Objects of SSTA by an Enhanced DcSTCA

With the time-series of a remote-sensing dataset, DcSTCA first uses spatial connectivity and the time evolution of marine anomaly variation to construct a spatiotemporal grid cube and then determines the spatiotemporal neighborhood. Within the spatiotemporal neighborhood, DcSTCA calculates the proximities in space, time, and thematic attributes in order to obtain spatiotemporal clustering cores and the spatiotemporal density of each grid cell [20]. In DcSTCA, there are three key parameters, i.e., the spatial neighborhood size, temporal evolution window, and core density threshold, which determine the final spatiotemporal clusters, and the setting of the temporal variation window is related to the determination of ENSO events. Taking the proximity in space, continuity in time, and the homogeneity in the thematic attributes into account, DcSTCA derives spatiotemporal clustering patterns of SSTA.

Thus, this paper first extracts spatiotemporal clusters of SSTA based on DcSTCA. Here, the spatial neighborhood size, temporal variation window, and core density threshold are set to 8 grid cells, 2 months and 15, respectively, which perform well in the Pacific Ocean [20]. Then, the Node Searching method [32] is used to vectorize the spatiotemporal cluster of SSTA at each time snapshot to polygons (objects)—that is, each cluster has grid cells at a time snapshot that are transformed into one snapshot object of SSTA.

2.2. Determining an Optimal Linking Threshold to Construct Process Objects of SSTA

While the clustering patterns of SSTA include all the SSTA that have similar spatiotemporal/thematic characteristics, there is no evolution between SSTA, and not all of them are generated from one process object. Only snapshot objects of SSTA in the previous/current/next time snapshots meet for a certain degree of the overlapped area belonging to a process object [25,26,31]. Thus, the degree of overlap area between snapshot objects is an important parameter to generate a process object.

The degree of overlap area (DOA) is calculated by Formula (1), where O_t and O_{t+1} represent snapshot objects at t and $t+1$ time snapshots, $Area(O_t)$ and $Area(O_{t+1})$ represent

the spatial covered area of O_t and O_{t+1} , and the $OverlappedArea(O_t, O_{t+1})$ represents an overlap area between O_t and O_{t+1} .

$$\begin{cases} DOA = DOA_t + DOA_{t+1} \\ DOA_t = \frac{OverlappedArea(O_t, O_{t+1})}{Area(O_t)} \\ DOA_{t+1} = \frac{OverlappedArea(O_t, O_{t+1})}{Area(O_{t+1})} \end{cases} \quad (1)$$

From Formula (1), the larger the DOA , the less snapshot objects of SSTA are generated into one process object, and the more small snapshot objects are omitted, and vice versa. Thus, how to determine an optimal linking threshold based on DOA is a key issue. As has already been established, DOA is greater or less than the threshold, and the number of overlap snapshot objects of SSTA will dramatically decrease or increase. Based on this precondition, PoAIES uses the geostatistics of all overlap snapshot objects of SSTA to automatically calculate the optimal threshold, denoted as Th_{DOA} . Additionally, Algorithm 1 shows the automatic calculation of Th_{DOA} .

Algorithm 1

Step1: Go through all overlap snapshot objects of SSTA, and calculate their DOA using Formula (1);

Step2: Sort the $DOAs$ by an increasing order, and draw its curve;

Step3: Find the inflection point of the curve, and the corresponding DOA is an optimal linking threshold, Th_{DOA} ;

Step4: Output the Th_{DOA} .

Similarly, the optimal linking threshold at time snapshot t , denoted as Th_{DOA}^t , is also automatically calculated. When optimal linking thresholds (Th_{DOA}, Th_{DOA}^t) are determined, snapshot objects of SSTA in successive snapshots t and $t+1$, meeting Inequalities (2) or (3), are linked together, then all snapshot objects of SSTA are generated

$$DOA \geq Th_{DOA} \quad (2)$$

$$DOA_t \geq Th_{DOA}^t \wedge DOA_{t+1} \geq Th_{DOA}^t \quad (3)$$

into process objects.

2.3. Graph-Based Representation on Process Objects

After the connection between snapshot objects is established, a process object is formed, but the connection itself lacks meaning, which is the evolution relationship type of connection. From the definition of the evolution relationship, it can be inferred that the meaning of the connection between two snapshot objects is determined by all the connections they involve. In order to simplify the problem, we use the graph to express the process object. $G(N, E)$ is the formal expression of a graph [33], where N represents a node, storing a snapshot object of SSTA, and E represents an edge, storing an evolution relationship between two snapshot objects of SSTA. In $G(N, E)$, an edge links two nodes, the starting node of an edge is named the parent node, and the ending node of an edge is named the child node. For example, Figure 2 shows a graph-based process object, and in the black dot rectangle, there are five evolution relationships between t_3 and t_4 , four parent nodes at t_3 , and three child nodes at t_4 . Among them, $Node_1$ and $Node_2$ are parent nodes of $Node_5$, $Node_3$ is a parent node of $Node_6$ and $Node_7$, and $Node_4$ is a parent node of $Node_7$. In reverse, $Node_5$ is a child node of $Node_1$ and $Node_2$, $Node_6$ is a child node of $Node_3$, and $Node_7$ is a child node of $Node_3$ and $Node_4$.

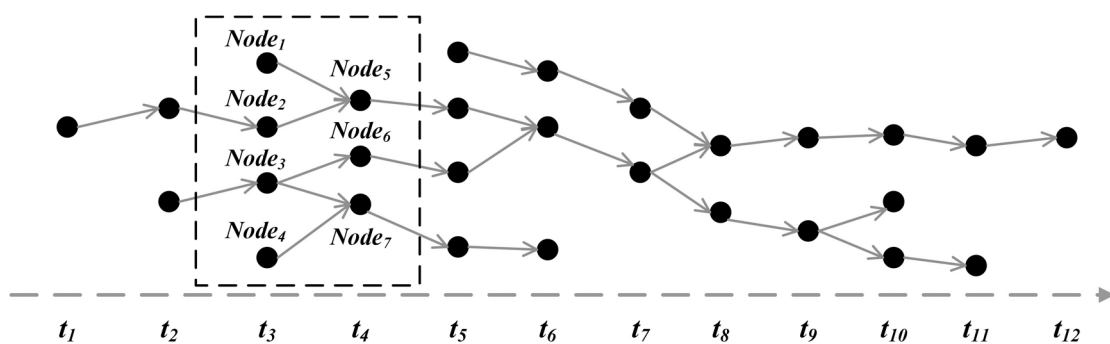


Figure 2. A schematic diagram of a graph-based process object.

The problem with regard to the meaning of the connection between two snapshot objects involving multiple connections, when using a graphical representation of process objects, can be transformed into the relationship between the out degree of the parent node and the in degree of the child node. This can bring great convenience to the identification of evolution relationships.

2.4. Identifying Evolution Relationships from Process Objects

From the graph-based process objects, there is a straightforward way to identify four types of evolution relationships between two nodes (a parent node and a child node). However, many false evolution relationships among process objects of SSTA generated only by the overlap area thresholds exist. The reasons are that a large amount of snapshot objects of SSTA that are too small and too large coexist at the same time snapshot. According to the evolution characteristics of SSTA, it is unrealistic that two and more snapshot objects of SSTA merge into one small object at the next time snapshot and that one small snapshot object of SSTA splits into two and more large objects. Figure 3 shows examples of false splitting and merging relationships. Thus, before identifying the real evolution relationships, we need to remove false evolutions and then reconstruct the process objects. This is an iterative loop. Figure 4 provides the iterative workflow for identifying evolution relationships from process objects.

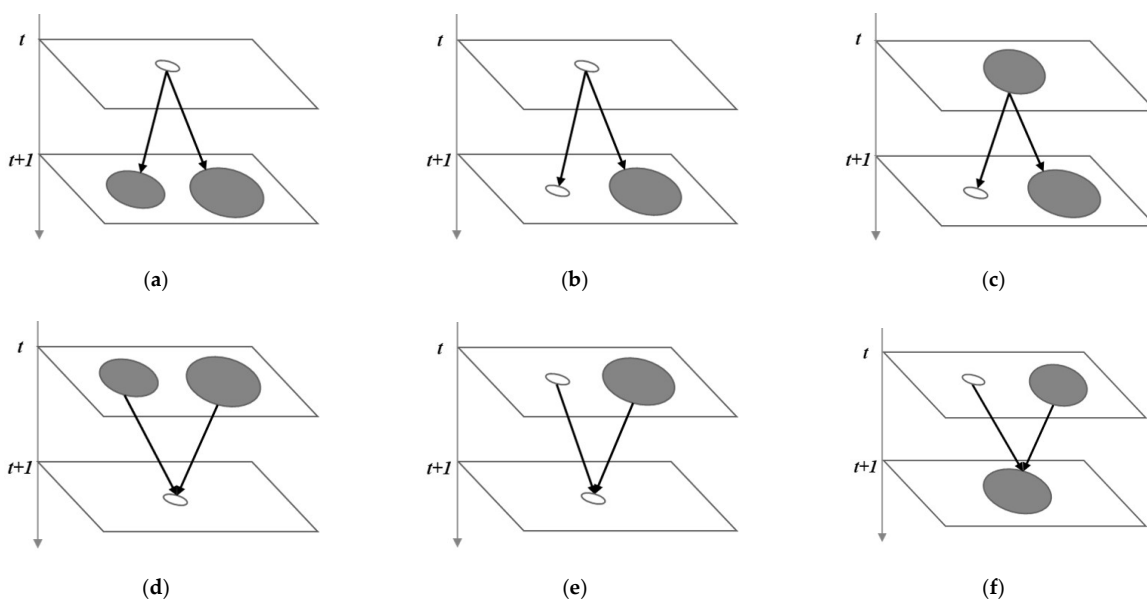


Figure 3. A diagram of false evolution relationships. (a–c) are false splitting relationships, and (d–f) are false merging relationships.

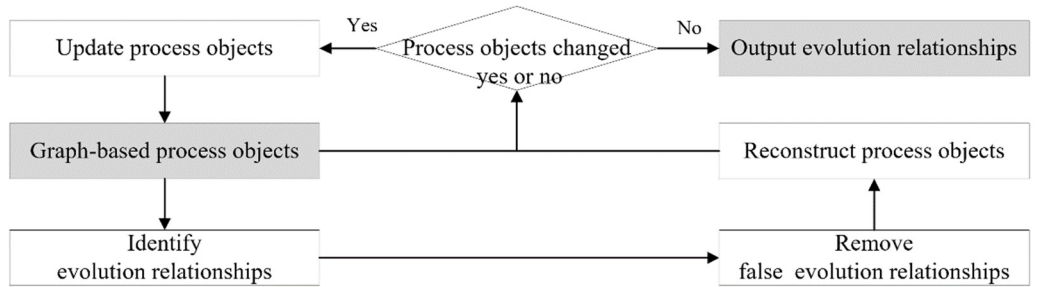


Figure 4. An iterative workflow to identify evolution relationships.

In Figure 4, an input is a graph-based process object, and outputs are four types of evolution relationships. Within the workflow, there are two key points, i.e., how to remove false evolution relationships and how to identify true evolution relationships.

2.4.1. Remove False Evolution Relationships

As has been established, a snapshot object of SSTA merging with another snapshot object at time t will strengthen the snapshot object at time $t+1$ in space or thematically. Similarly, a snapshot object of SSTA splits into two and more snapshot objects at time t , and each split object at time $t+1$ will weaken in space or thematically. This paper regards such an evolution relationship as going against the above knowledge, meaning that it can be considered as the first kind of false evolution relationship, as shown in Figure 3a,b,d,e. The second kind of false evolution relationship is in that a snapshot object of SSTA splits into many objects in the next time snapshot, and sometimes these split objects are not of the same order of magnitude in space, as shown in Figure 3c. Similarly, the snapshot objects of SSTA being merged in the next time snapshot are also not of the same order in space, as shown in Figure 3f. Such evolution relationships may be true, but to simplify the graph-based process objects of SSTA and to further analyze their dynamics, this paper also regards these splitting and merging relationships as false ones.

To remove the first kind of false evolution relationship, this paper combines the spatial coverage area and thematic value of the snapshot objects of SSTA as parameters in order to define a splitting degree (SD) and a merging degree (MD), and their calculations are shown Formulas (4) and (5). Additionally, the relative importance of splitting or merging objects in space and thematically is intended to remove the second kind of false evolution relationship, and their calculations are given in Formulas (6) and (7).

$$SD = \left\{ SD^i \middle| SD^i = \frac{\text{Area}(O_{t+1}^i) * \text{Attr}(O_{t+1}^i)}{\text{Area}(O_t) * \text{Attr}(O_t)} \right\}, (i = 2 \dots N) \quad (4)$$

$$MD = \left\{ MD^i \middle| MD^i = \frac{\text{Area}(O_t^i) * \text{Attr}(O_t^i)}{\text{Area}(O_{t+1}) * \text{Attr}(O_{t+1})} \right\}, (i = 2 \dots N) \quad (5)$$

$$RI_S(E) = \frac{\text{Area}(O_{t+1}^i) * \text{Attr}(O_{t+1}^i)}{\max\{\text{Area}(O_{t+1}^i) * \text{Attr}(O_{t+1}^i)\}}, (i = 2 \dots N) \quad (6)$$

$$RI_M(E) = \frac{\text{Area}(O_t^i) * \text{Attr}(O_t^i)}{\max\{\text{Area}(O_t^i) * \text{Attr}(O_t^i)\}}, (i = 2 \dots N) \quad (7)$$

where $\text{Area}(O_t)$ and $\text{Attr}(O_t)$ represent a spatial coverage area and a thematic value of a snapshot object (O) at time t , and $\text{Area}(O_t^i)$ and $\text{Attr}(O_t^i)$ represent a spatial coverage area and a thematic value of the i th snapshot object (O) at time t . N is a number of split objects at time $t+1$ in Formulas (4) and (6) and is a number of objects at time t that will be merged at time $t+1$ in Formulas (5) and (7).

Generally, these kinds of false evolution relationships are far less than the normal ones—that is, a number of false relationships will dramatically decrease/increase when $MD/SD/RI_S(E)/RI_M(E)$ is greater/less than a threshold of $MD/SD/RI_S(E)/RI_M(E)$, denoted as $Th_{SD}/Th_{MD}/Th_{RI_S}/Th_{RI_M}$. Based on this precondition, this paper automatically calculates the optimal $Th_{SD}/Th_{MD}/Th_{RI_S}/Th_{RI_M}$ using Algorithm 2.

Algorithm 2

Step1: From the graph –

based process objects, obtain all matched parent nodes and child nodes through splitting/merging edges, and calculate their $SD/MD/RI_S(E)/RI_M(E)$ using Formula (4)/ Formula (5)/ Formula (6)/ Formula (7);

Step2: Sort the $SD/MD/RI_S(E)/RI_M(E)$ by an increasing order, and draw its curve;

Step3: Find an inflection point of the $SD/MD/RI_S(E)/RI_M(E)$ curve, and a corresponding value of $SD/MD/RI_S(E)/RI_M(E)$ is an optimal threshold, $Th_{SD}/Th_{MD}/Th_{RI_S}/Th_{RI_M}$;

Step4: Output the $Th_{SD}/Th_{MD}/Th_{RI_S}/Th_{RI_M}$.

When the optimal thresholds, $Th_{SD}, Th_{MD}, Th_{RI_S}$ and Th_{RI_M} , were obtained, this paper used Inequality (8) to remove the second kind of false evolution relationships, and then Inequality (9) was used to remove the first kind of false evolution relationships.

$$\begin{cases} RI_S(E) < Th_{RI_S} \\ RI_M(E) < Th_{RI_M} \end{cases} \quad (8)$$

$$\begin{cases} SD > Th_{SD} \\ MD > Th_{MD} \end{cases} \quad (9)$$

2.4.2. Identify True Evolution Relationships

In a graph-based model, an edge represents an evolution relationship, and two nodes linking the edge represent snapshot objects of SSTA at time snapshots t and $t+1$. According to the above-mentioned definition of four types of evolution relationships, this paper uses a number of child nodes of an edge's parent node and a number of parent nodes of the edge's child node. The straight identification is shown in Table 1.

Table 1. Identification of four types of evolution relationships.

Evolution Relationship	Rule
<i>Development</i> ($Object_t, Object_{t+1}$)	The out degree of $Node_t$ and the in degree of $Node_{t+1}$ are both 1. $NumofChildNodes(Node_t) = 1$ $\wedge NumofParentNodes(Node_{t+1}) = 1$
<i>Splitting</i> ($Object_t, Object_{t+1}$)	The out degree of $Node_t$ is greater than 1 and the in degree of $Node_{t+1}$ is 1. $NumofChildNodes(Node_t) > 1$ $\wedge NumofParentNodes(Node_{t+1}) = 1$
<i>Merging</i> ($Object_t, Object_{t+1}$)	The out degree of $Node_t$ is 1 and the in degree of $Node_{t+1}$ is greater than 1. $NumofChildNodes(Node_t) = 1$ $\wedge NumofParentNodes(Node_{t+1}) > 1$
<i>Splitting/merging</i> ($Object_t, Object_{t+1}$)	The out degree of $Node_t$ and the in degree of $Node_{t+1}$ are both greater than 1. $NumofChildNodes(Node_t) > 1$ $\wedge NumofParentNodes(Node_{t+1}) > 1$

In Table 1, $Object_t$ and $Object_{t+1}$ are snapshot objects of SSTA at time t and $t+1$, corresponding to the nodes $Node_t$ and $Node_{t+1}$. $NumofChildNodes(Node_t)$ represents a number

of child nodes of an edge's parent node ($Node_t$), and $NumofParentNodes(Node_{t+1})$ represents a number of parent nodes of the edge's child node ($Node_{t+1}$).

3. Experiments and Evaluations

3.1. Simulated Dataset and Performance Analysis

3.1.1. Simulated Dataset

To evaluate PoAIES, we simulated 20 process objects and some random noises, and their temporal and spatial distributions are shown in Figure 5. The simulated datasets lasted for 20 time snapshots and included 235 snapshot objects, 23 random noise objects, 188 evolution relationships, and 36 false evolution relationships; their detailed information is shown in Table 2. In the simulated datasets, the minimum duration of a process object was five time snapshots; otherwise, it was considered to be noise.

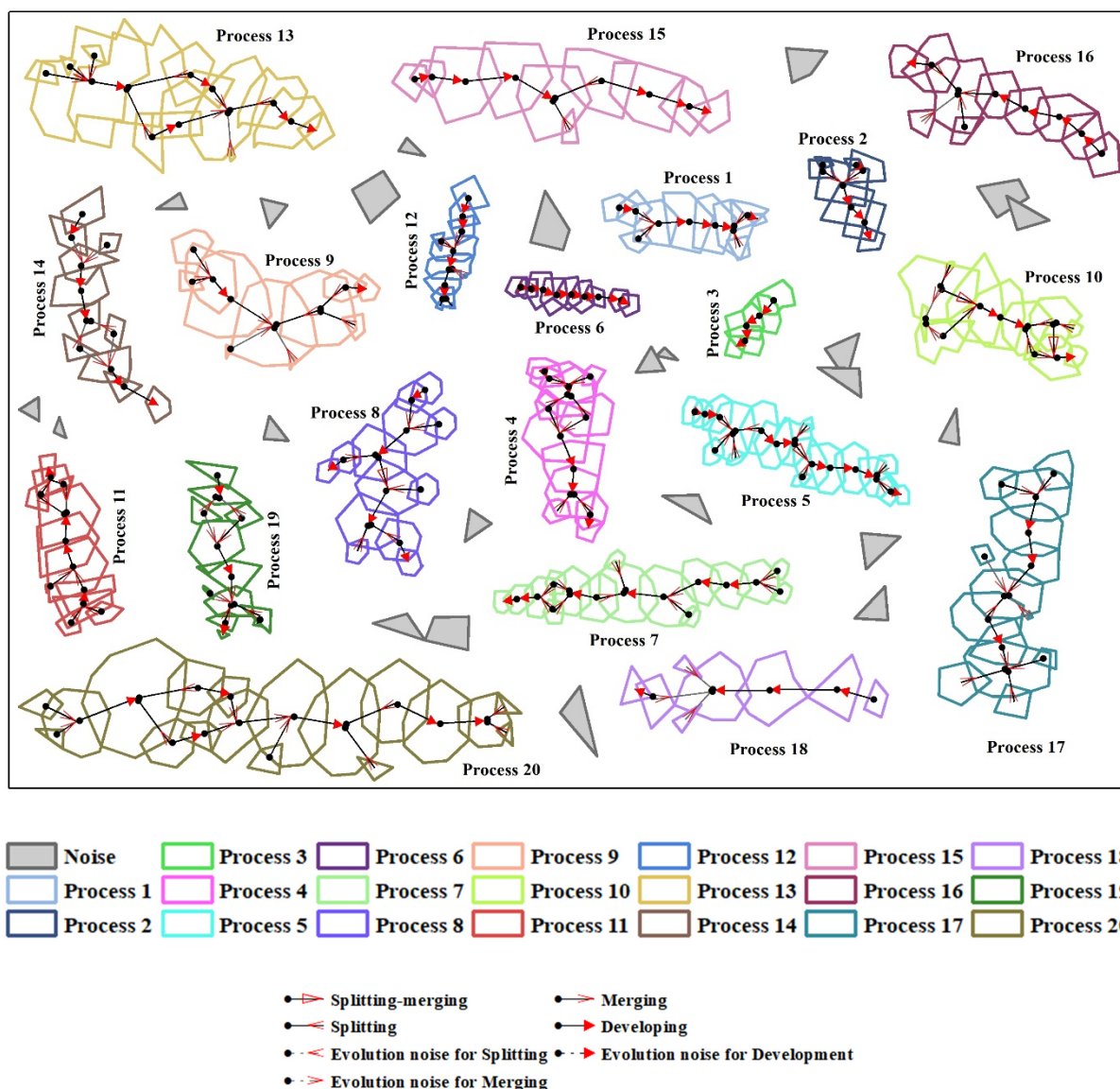


Figure 5. Simulated datasets of process objects and noises.

Table 2. Details of the simulated datasets. *ProcessID*, *Stime*, *Etime*, and *Nums* are a unique identifier, a start time, an end time, and a number of snapshot objects consisting of a process object, respectively.

ProcessID	Stime	Etime	Nums	Number of Evolution Relationships			
				Development	Merging	Splitting	Splitting/Merging
1	t_1	t_8	10	5	2	2	0
2	t_3	t_8	8	5	2	0	0
3	t_2	t_6	5	4	0	0	0
4	t_5	t_{14}	13	5	4	4	0
5	t_1	t_{13}	18	8	3	5	1
6	t_7	t_{15}	9	8	0	0	0
7	t_4	t_{15}	16	6	6	4	0
8	t_7	t_{14}	13	5	3	3	1
9	t_{10}	t_{16}	11	2	4	4	0
10	t_{13}	t_{20}	12	3	2	6	2
11	t_9	t_{17}	12	4	6	2	0
12	t_{12}	t_{19}	11	4	2	4	0
13	t_{10}	t_{18}	14	5	5	4	0
14	t_{12}	t_{20}	11	5	4	2	0
15	t_{11}	t_{19}	10	7	0	2	0
16	t_{13}	t_{20}	10	5	2	2	0
17	t_{10}	t_{18}	14	3	6	4	0
18	t_{15}	t_{20}	8	4	0	3	0
19	t_9	t_{16}	12	4	4	4	0
20	t_8	t_{19}	18	6	6	6	0

3.1.2. Thresholds and Performances

Using Algorithm 1, PoAIES calculates the optimal linking threshold, $Th_{DOA} = 0.203$ and $Th_{DOA}^t = 0.051$. Figure 6 shows their calculating curves. All the snapshot objects meeting for the inequality $DOA > 0.203$, or the inequality $DOA_t > 0.051$ are generated into process objects.

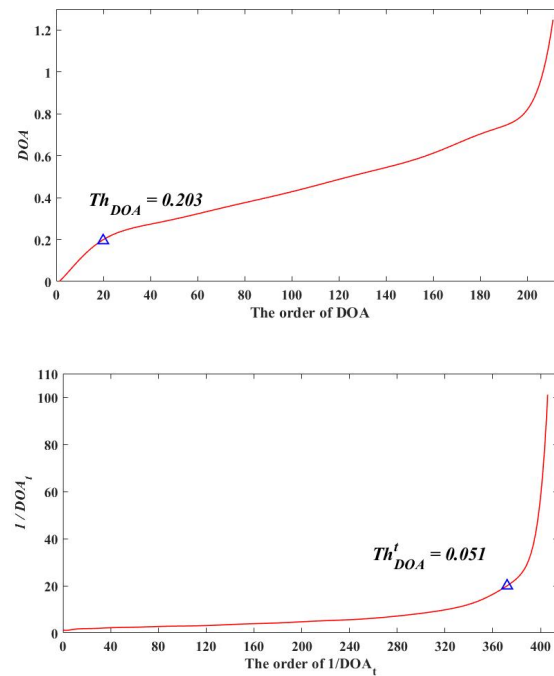


Figure 6. The calculation of linking thresholds. The triangle symbol is located at the inflection point of the curve, and the equation represents the value of the corresponding variable at the inflection point.

When process objects are generated, the evolution relationships are obtained from the graph-based process objects, and Algorithm 2 is used to remove false evolution relationships. Figure 7 shows curves to determine optimal splitting thresholds, $Th_{SD} = 1.514$ and $Th_{RI_S} = 0.083$, and Figure 8 shows curves to determine the optimal merging thresholds, $Th_{MD} = 1.320$ and $Th_{RI_M} = 0.069$. Thus, if one edge meets for the inequality $RI_S(E) < 0.083$ or the inequality $SD > 1.514$, its corresponding splitting relationship is false, and the edge will be deleted from the process object. Similarly, if one edge meets for the inequality $RI_M(E) < 0.069$, or the inequality $MD > 1.320$, the merging relationship is false, and the edge will also be deleted.

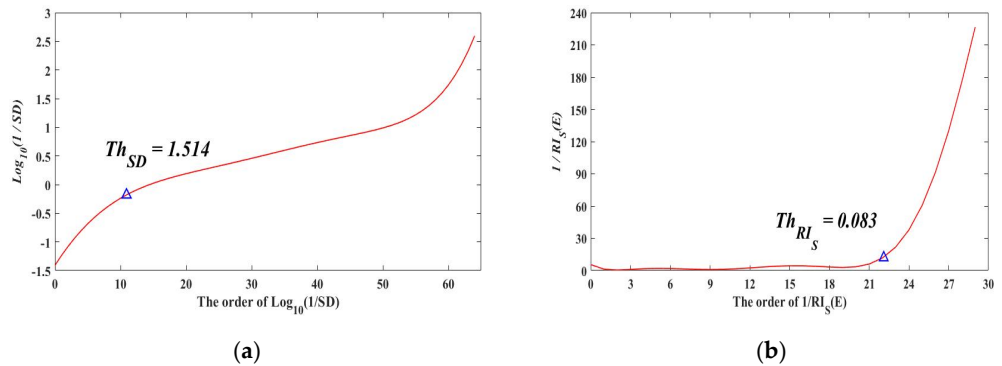


Figure 7. The optimal threshold of splitting evolution for the simulated dataset. The triangle symbol is located at the inflection point of the curve, and the equation represents the value of the corresponding variable at the inflection point. (a,b) are splitting degree and relative importance of split objects, respectively.

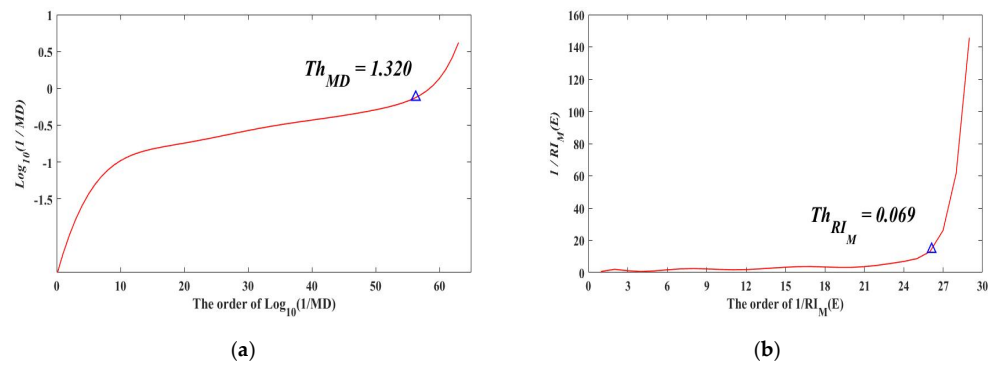


Figure 8. The optimal threshold of merging evolution for the simulated dataset. The triangle symbol is located at the inflection point of the curve, and the equation represents the value of the corresponding variable at the inflection point. (a,b) are merging degree and relative importance of being merged objects, respectively.

When all the splitting edges and merging edges are gone through, the false evolution relationships are deleted, and process objects are reconstructed into new ones. Additionally, a recursive removal of false evolution relationships is performed until the process objects are not changed, and then the final evolution relationships are obtained. Figure 9 shows the final process objects and their evolution relationships of the simulated datasets.

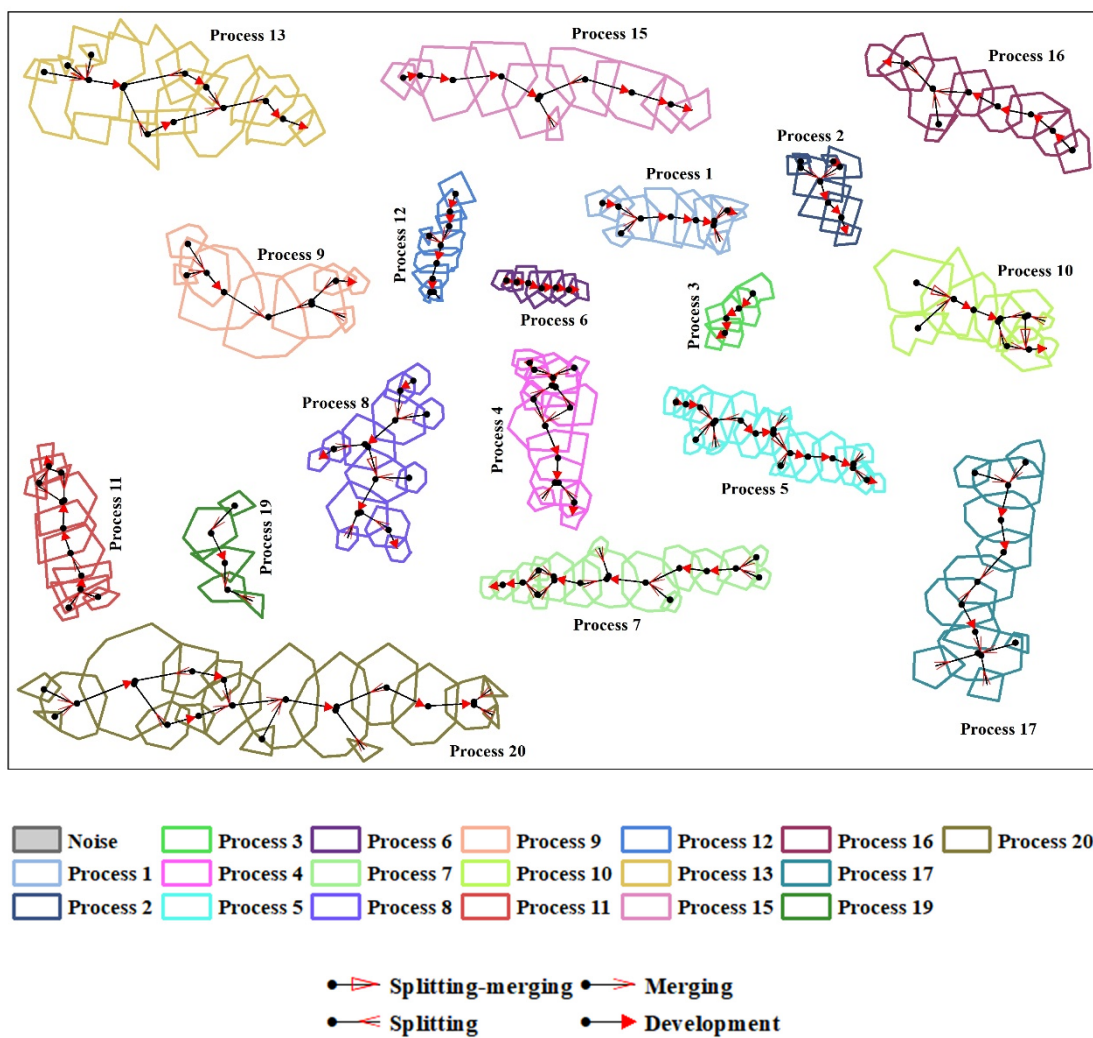


Figure 9. Final process objects and their evolution relationships of the simulated datasets.

From Figure 9, we know that 18 out of 20 process objects are obtained, which include 198 snapshot objects and 179 evolution relationships. As snapshot objects of Process 14 do not meet the linking thresholds from t_5 to t_6 , i.e., the durations of two obtained process objects are both less than five time snapshots; thus, Process 14 is not detected. Regarding Process 18, false splitting relationships from t_4 to t_5 exist, which are removed by the splitting threshold. After the duration of the generated process objects that are less than five time snapshots, Process 18 is also not detected.

To analyze the performance of PoAIES, this paper selects four evaluation indicators: accuracy, precision, recall, and an F1Score, which are computed by Equation (10):

$$\left\{ \begin{array}{l} \text{Accuracy} = \frac{TP+TN}{TP+FN+FP+TN} \\ \text{Precision} = \frac{TP}{TP+FP} \\ \text{Recall} = \frac{TP}{TP+FN} \\ \text{F1Score} = \frac{2*\text{Recall}*\text{Precision}}{\text{Recall}+\text{Precision}} \end{array} \right. \quad (10)$$

where TP is a number of true objects (snapshot object, process object, or evolution relationship) retrieved from true objects, FP is a number of false objects retrieved from true objects, FN is a number of noises that are regarded as true objects, and TN is a number of noises that are regarded as noises.

As shown in Table 3, the overall identifying capability of process objects is higher than that of snapshot objects. The reason lies in the random noise that is isolated, which

cannot make up for a process object; thus, no snapshot objects are identified as process objects. Further, the accuracy, precision, recall, and F1Score of the whole of the evolution relationships are all above 94%, which shows a high capability to identify the evolution relationships of PoAIES.

Table 3. Evaluations of snapshot objects, process objects, and evolution relationships.

	Accuracy	Precision	Recall	F1Score
Snapshot object	85.66	100.00	84.26	91.45
Process object	90.00	100.00	90.00	94.74
Evolution relationship	94.20	98.88	94.15	96.46

3.2. Dynamic Analysis of Process-Oriented SSTA Evolutions

3.2.1. A Remote-Sensing Dataset

The real dataset is the Level 3 monthly SST product provided by NASA/JPL/PO.DAAC, which was available at <https://podaac-tools.jpl.nasa.gov/drive/files/allData> (accessed on 22 July 2021) for the period from January 1982 to December 2018. The products were derived from MODIS and AVHRR, with spatial resolutions of 4.6 km and 4.9 km. The AVHRR dataset covers the period from January 1982 to December 2009, and the MODIS dataset covers the period from January 2002 to December 2018. Further, the standard monthly average anomaly algorithm, denoted as the *z-score* [34], was used to remove seasonal variations of SST that were mainly dominated by solar radiance, and the monthly SSTA dataset was generated to construct process objects.

To analyze the relationships between evolutions of SSTA and ENSO, MEI was used to characterize ENSO, and an MEI greater than 0.5 (less than −0.5) for at least 5 consecutive months was regarded as an occurrence of an El Niño (La Niña) event [35].

3.2.2. Process-Oriented Objects of SSTA and their Evolutions

When all the snapshot objects of SSTA were obtained by an enhanced DcSTCA, we used Formula (1) and Algorithm 1 to calculate the optimal linking thresholds, Th_{DOA} and Th_{DOA}^t , which is shown in Figure 10a,b. The successive snapshot objects meeting for one of two equalities, $DOA > 0.589$ and $DOA_t > 0.054$, were linked together. On the basis of graph-based process objects, Algorithm 2 was used to calculate an optimal relative importance threshold of split snapshot objects, $Th_{RI_S} = 0.126$, and a threshold of merged snapshot objects, $Th_{RI_D} = 0.137$, which are shown in Figure 10c,d. Additionally, the optimal splitting and merging thresholds are shown in Figure 10e,f.

We used $RI_S(E) < 0.126$ and $SD > 1.393$ to remove false splitting relationships, and $RI_M(E) < 0.137$ and $MD > 0.530$ to remove false merging relationships. Then, graph-based process objects of SSTA were reconstructed and final evolution relationships were identified. Finally, we obtained 208 process objects of SSTA, which included 4036 snapshot objects of SSTA and 3523 evolution relationships. According to the thematic value of SSTA, the process objects were categorized into two classes: a warm process object (the value of SSTA greater than zero) and a cold one (the value of SSTA less than zero). The details of the process objects of SSTA are shown in Table 4, and their spatial coverage is shown in Figure 11.

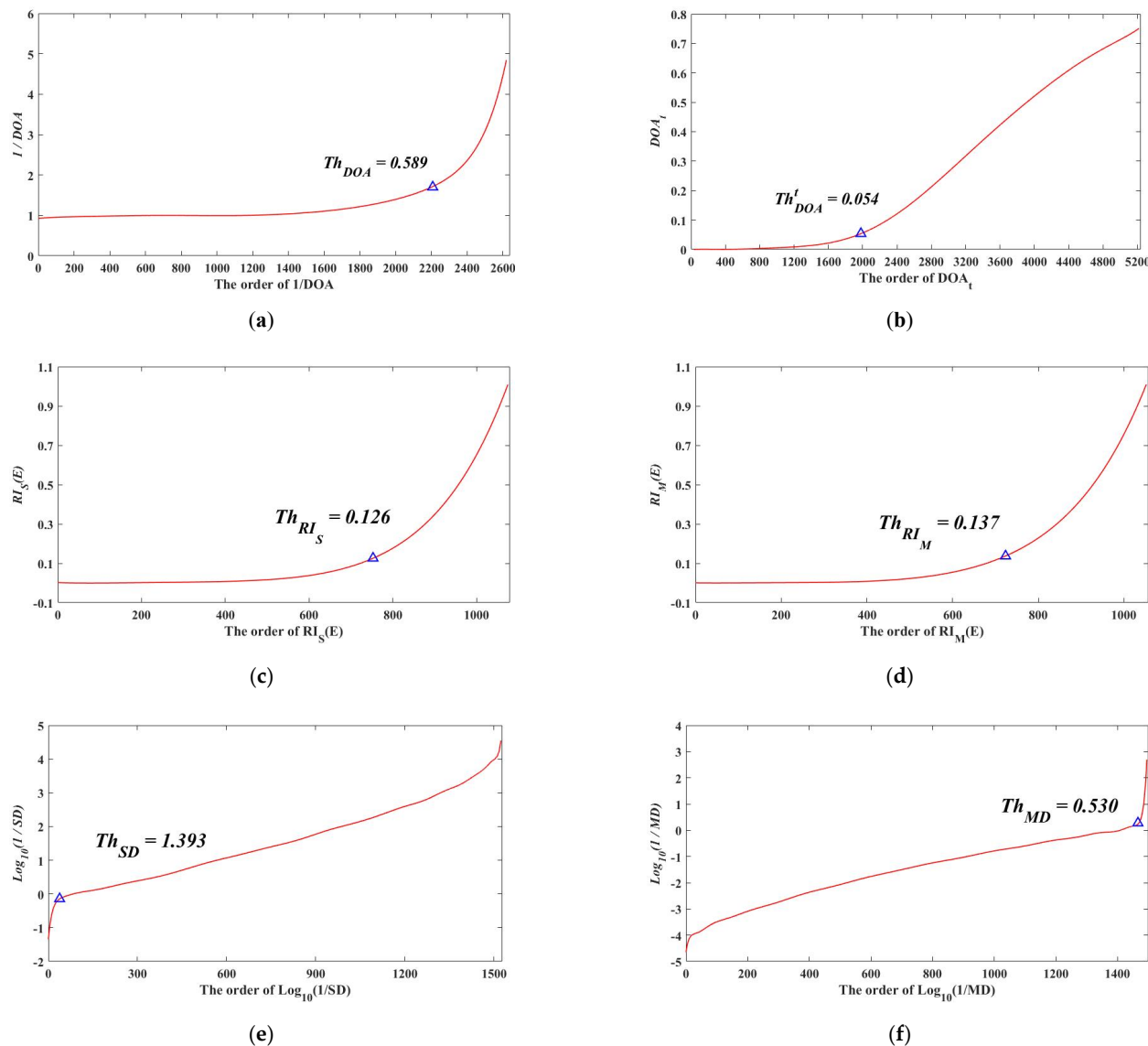


Figure 10. Parameter thresholds at different stages. The triangle symbol is located at the inflection point of the curve, and the equation represents the value of the corresponding variable at the inflection point. (a,b) are the linking thresholds of snapshot objects of SSTA, (c,d) are relative importance thresholds of snapshot objects of SSTA, and (e,f) are splitting/merging degree thresholds between the matched parent–child nodes (objects of SSTA at snapshots t and $t + 1$). In addition, (a,b) represent a sum of DOA and a DOA at a time snapshot, respectively. Both (c) and (e) are splitting situation. Both (d) and (f) are merging situation.

Table 4. Details of the process objects of SSTA.

Type	No. of Process Objects	No. of Snapshot Objects	Evolution Relationship	
			Type	Num
Warm	122	2701	<i>Development</i>	1510
			<i>Splitting</i>	388
			<i>Merging</i>	417
			<i>Splitting/merging</i>	12
Cold	86	1335	<i>Development</i>	751
			<i>Splitting</i>	215
			<i>Merging</i>	220
			<i>Splitting/merging</i>	10

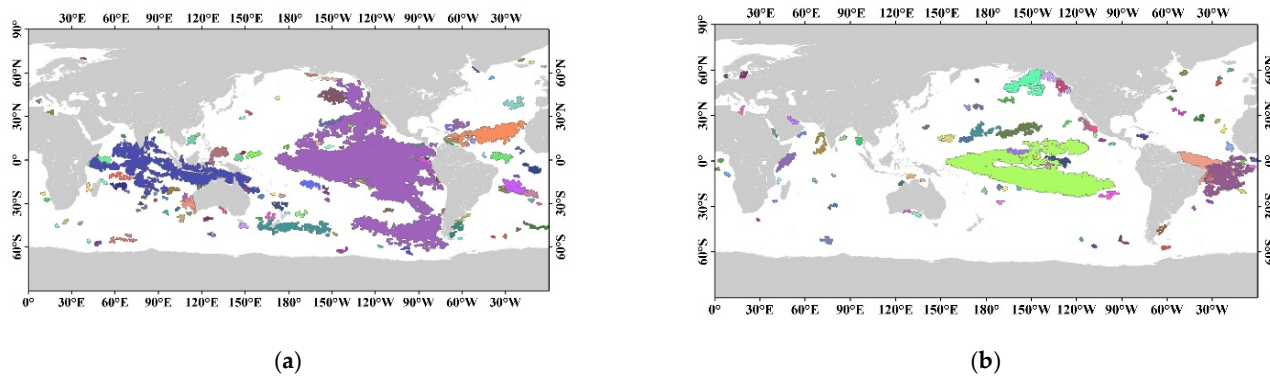


Figure 11. Spatial coverage of the process objects of SSTA. Different colors denote different process objects. (a,b) are warm process objects and cold process objects, respectively.

3.2.3. Relationships between SSTA Evolutions and ENSO

To describe the strength of a process object at each time snapshot, we took a product of an area and a thematic value of a snapshot object of SSTA as a process intensity, which were calculated and standardized using Formula (11).

$$\left\{ \begin{array}{l} NPI_t = \frac{PI_t - \text{Average}(PI)}{\text{Std}(PI)} \\ PI_t = \text{Area}(PO_t) * \text{Attr}(PO_t) \\ \text{Std}(PI) = \sqrt{\frac{\sum_{t=1}^{DT} (PI_t - \text{Average}(PI))^2}{DT-1}} \\ \text{Average}(PI) = \frac{\sum_{t=1}^{DT} PI_t}{DT} \end{array} \right. \quad (11)$$

where DT is the duration time of a process object, $\text{Area}(PO_t)$ and $\text{Attr}(PO_t)$ are the area and a thematic value of a snapshot object of SSTA at time snapshot t , $\text{Std}(PI)$ and $\text{Average}(PI)$ are a standard deviation and an averaged value of a process object intensity, and PI_t and NPI_t are a process object intensity and a normalized process object intensity at time snapshot t .

In this paper, we assumed that the intensity of ENSO was represented by an index (MEI)—that is, ENSO is strengthened when its index increases and is weakened when its index decreases. Its strength or weakness has a close relationship with SSTA in the Pacific Ocean. Table 5 provides statistics of the evolution relationship of all process objects of SSTA that occurred in the Pacific Ocean and their corresponding development stage of ENSO (a strengthening or a weakening) during the period of January 1982 to December 2018, showing that the merging/splitting evolution of the process objects of SSTA will strengthen/weake. nNSO with a high probability.

Table 5. Relationships between the development of ENSO with an evolution of SSTA. Warm SSTA refers to El Niño and cold SSTA to La Niña.

Type of SSTA	Development Stage of ENSO	Evolution Relationship of Process Object	
		Merging	Splitting
Warm	Strengthening	83.87%	16.13%
	Weakening	24.58%	75.42%
Cold	Strengthening	85.11%	14.89%
	Weakening	27.35%	72.65%

Different types of ENSO, i.e., EP ENSO and CP ENSO, occur, and where and how the SSTA evolves are different [36,37]. In regard to this issue, we assumed that all development, merging, and splitting relationships of the process objects of SSTA occurred in the Pacific

Ocean during EP ENSO, and we analyzed their dynamics in space. Figure 12 provides the evolution frequencies occurring in space.

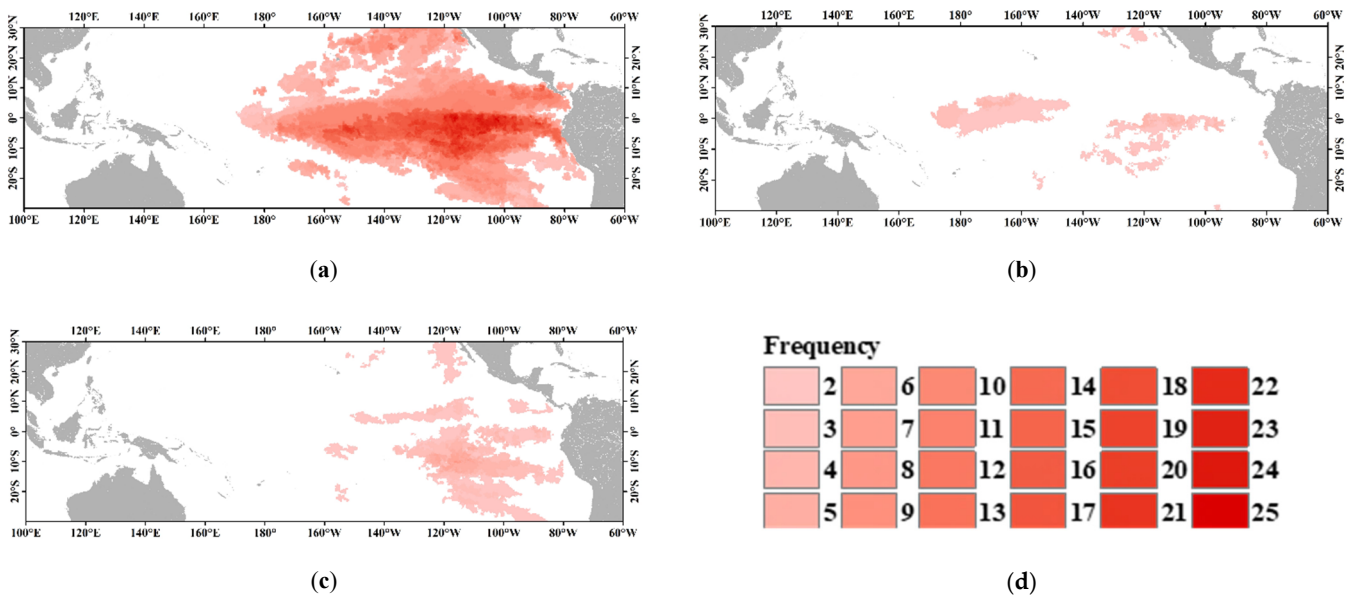


Figure 12. Spatial frequencies of the evolution relationships of warm process objects of SSTA during EP ENSO. (a–d) are development, merging, splitting, and legend.

From Figure 12, SSTA originates in the Eastern Pacific Ocean and then extends to the west during the westward period, and SSTA begins to strengthen by merging until it becomes the strongest in the Central Pacific Ocean, before turning to the east and then beginning to weaken by splitting until it dies in the Eastern Pacific Ocean. The evolution of the process objects of SSTA from eastern to central and then to the Eastern Pacific Ocean is consistent with SSTA characteristics caused by EP ENSO [38,39]. Figures 13 and 14 show an evolution in space and time of the process object of SSTA occurring from 1982 to 1983 and their relationships with corresponding EP El Niño.

In Figure 13, the process object of SSTA originates in the Central and Eastern Pacific Ocean and then gradually extends to the west and south. SSTA merged frequently before January 1983, and their spatial coverage reached its maximum in February 1983. After the process object moves eastward, during this period, it continues to split until it disappears in the Central or Eastern Pacific Ocean. Figure 14 shows that the merging/splitting evolutions of SSTA strengthens/weaken the process object and has a close relationship with EP El Niño. For example, in December 1982, some snapshot objects of SSTA merged into one object, and the intensity of the process object increased dramatically. Meanwhile, the index of El Niño continued to increase. In April and May 1983, one snapshot object of SSTA continued to split into more snapshot objects, which decreased the intensity of the process object, and at the same time, the index of El Niño began to decrease dramatically until it disappeared.

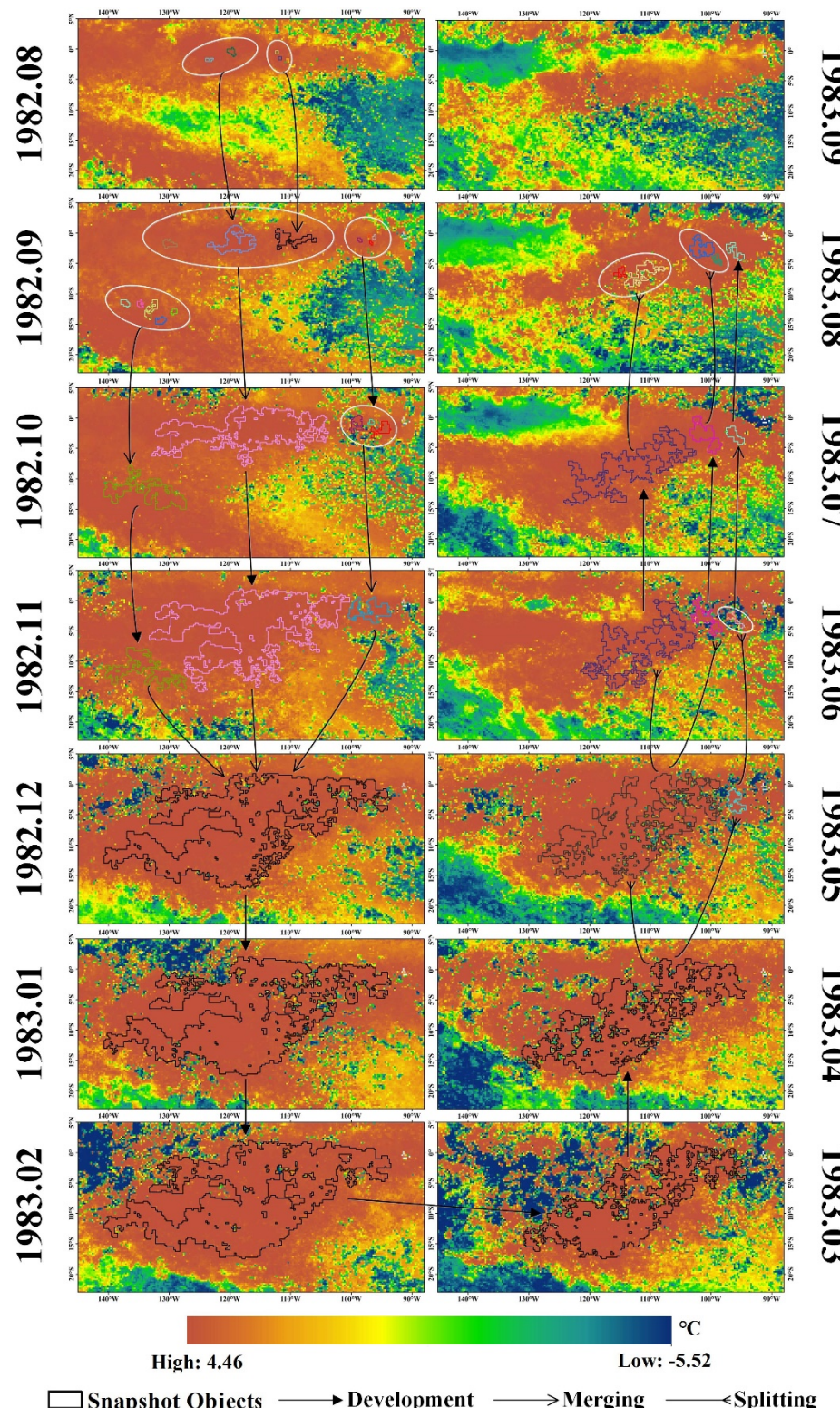


Figure 13. An evolution of the process objects of SSTA during the period from 1982 to 1983 in the Pacific Ocean. The snapshot objects contained in the white circle are divided into two situations: (1) merging at the next moment and (2) splitting from the previous moment.

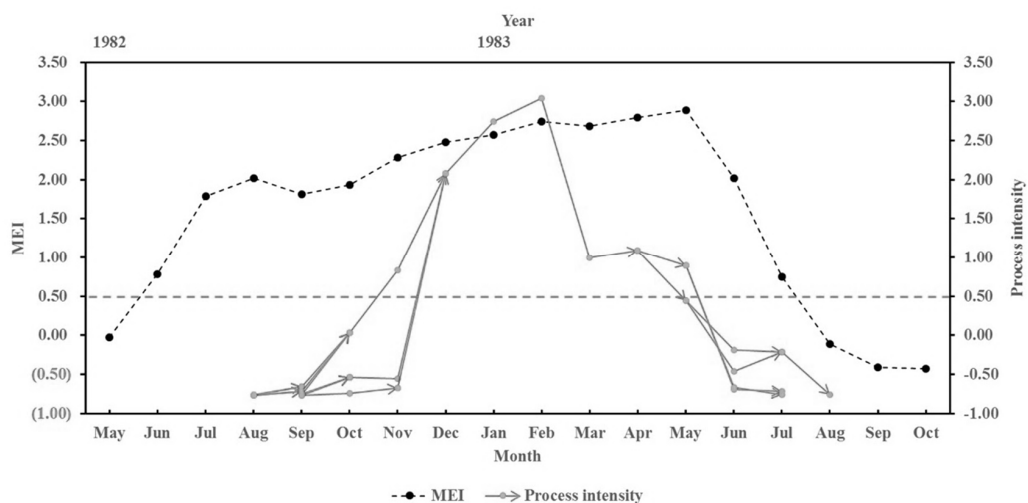


Figure 14. An evolution of the process objects of SSTA and its relationship with ENSO.

4. Conclusions

It is important to understand where, when, and how SSTA variation and evolution may be a driver or a responder to regional extreme climate events such as ENSO. To address such dynamics of SSTA in space and time, this paper designed PoAIES in order to obtain process objects of SSTA from a long time-series from a remote-sensing dataset, which included snapshot objects and their evolution relationships. Furthermore, a simulated dataset and a real dataset retrieved from a remote-sensing dataset in the Pacific Ocean were evaluated in order to prove the effectiveness and feasibility of PoAIES. The main conclusions are as follows.

(1) In view of the evolution from generation to development and dissipation, we designed PoAIES in order to obtain the process objects of SSTA, which not only obtained snapshot objects of SSTA but also their evolutions among successive snapshots. In PoAIES, two issues were addressed. One used the overlapped area of snapshot objects between successive time snapshots to automatically find the optimal linking threshold and linked the successive snapshot objects into a process object. The other considered evolving characteristics of SSTA in space and time in order to calculate the optimal splitting and merging thresholds and then removed the false splitting and merging evolution relationships. In comparison to a subject threshold, the data-driven threshold performed more suitably, which was proven by the simulated dataset.

(2) A graph-based model was proposed to express process objects of SSTA, i.e., a node representing a snapshot object, and an edge representing an evolution relationship. According to the number of parent nodes of an edge's child node and the number of child nodes of the edge's parent node, a type of edge between two nodes was straightly obtained. Thus, four kinds of evolution relationships were obtained: development, splitting, merging, and splitting/merging.

(3) Twenty process objects, including 235 snapshot objects and 188 evolution relationships and noises, were simulated to validate the PoAIES. A high level of accuracy, precision, recall, and F1Score of the snapshot objects and evolution relationship shows that PoAIES has the capability of obtaining process objects. While the linking threshold and the splitting/merging threshold are determined automatically, they also affect the capacity to obtain them. For example, the linking thresholds with $DOA > 0.203$ and $DOAT > 0.051$ removed the real snapshot object at T4 from the process object 17 (Process 17); thus, two merging relationships transformed into one development relationship, which reduced the obtaining capability of PoAIES.

(4) We obtained 208 process objects of SSTA using the remote-sensing datasets during the period from January 1982 to December 2018 and found that the merging/splitting evolution of the process objects of SSTA would strengthen/weaken ENSO intensity with

a high probability. Additionally, the spatial distribution and migration of development, merging, and splitting relationship may provide a new reference to identify different types of ENSOs, i.e., EP ENSO and CP ENSO. The association relationships between ENSO types and evolutions of SSTA in space and time require further study.

PoAIES can effectively extract the inherent evolutionary relationship of SSTA spatiotemporal clusters, which is helpful for more in-depth research and in the analysis of SSTA change patterns. However, the core of PoAIES is the spatiotemporal topology, and due to the low time resolution of the dataset, snapshot objects with a small coverage area are completely likely to disappear and regenerate within a month, which will cause the results to deviate from the real value, so the time resolution of the dataset applied to the PoAIES should not be too low. In addition, evolution relationships not only represent the connection between the snapshot objects but also indicate the movement trajectory of SSTA and the flow direction of ocean currents; therefore, in the future, the role of the ocean current's field can be considered when making the connection between snapshot objects, which is not only helpful to improve the accuracy of results but can also alleviate the dependence of PoAIES on the time resolution of the dataset.

Author Contributions: Conceptualization, Lianwei Li and Cunjin Xue; Data curation, Yangfeng Xu; Formal analysis, Yangfeng Xu; Funding acquisition, Cunjin Xue; Methodology, Lianwei Li; Project administration, Cunjin Xue; Software, Yangfeng Xu; Validation, Yuxuan Fu and Yuanyu Zhang; Writing—original draft, Lianwei Li; Writing—review & editing, Cunjin Xue. All authors have read and agreed to the published version of the manuscript.

Funding: This research was jointly supported by Strategic Priority Research Program of the Chinese Academy of Sciences with Grant No. XDA19060103, and the Fundamental Research Funds for the Central Universities with Grant No. 17CX02005A, and the National Natural Science Foundation of China with Grant Nos. 41976184 and 41671401.

Institutional Review Board Statement: Not applicable.

Informed Consent Statement: Not applicable.

Data Availability Statement: The datasets generated and analyzed during the current study are available from the corresponding author on reasonable request.

Acknowledgments: We thank the NASA/JPL/PO.DAAC for providing the research data.

Conflicts of Interest: The authors declare no conflict of interest.

References

1. Hollmann, R.; Merchant, C.; Saunders, R.; Downy, C.; Buchwitz, M.; Cazenave, A.; Chuvieco, E.; Defourny, P.; De Leeuw, G.; Forsberg, R.; et al. The ESA Climate Change Initiative: Satellite Data Records for Essential Climate Variables. *Bull. Am. Meteorol. Soc.* **2013**, *94*, 1541–1552. [[CrossRef](#)]
2. Murtugudde, R.; Wang, L.; Hackert, E.; Beauchamp, J.; Christian, J.; Busalacchi, A.J. Remote sensing of the Indo-Pacific region: Ocean colour, sea level, winds and sea surface temperatures. *Int. J. Remote Sens.* **2004**, *25*, 1423–1435. [[CrossRef](#)]
3. Dai, A. Future Warming Patterns Linked to Today's Climate Variability. *Sci. Rep.* **2016**, *6*, 19110. [[CrossRef](#)]
4. Xue, C.J.; Song, W.J.; Qin, L.J.; Dong, Q.; Wen, X. A spatiotemporal mining framework for abnormal association patterns in marine environments with a time series of remote sensing images. *Int. J. Appl. Earth Obs. Geoinf.* **2015**, *38*, 105–114. [[CrossRef](#)]
5. McPhaden, M.J.; Zebiak, S.E.; Glantz, M.H. ENSO as an Integrating Concept in Earth Science. *Science* **2006**, *314*, 1740–1745. [[CrossRef](#)]
6. McGregor, S.; Timmermann, A.; Schneider, N.; Stuecker, M.F.; England, M.H. The Effect of the South Pacific Convergence Zone on the Termination of El Niño Events and the Meridional Asymmetry of ENSO. *J. Clim.* **2012**, *25*, 5566–5586. [[CrossRef](#)]
7. Ashok, K.; Behera, S.; Rao, S.A.; Weng, H.; Yamagat, H.W.A.T. El Niño Modoki and its possible teleconnection. *J. Geophys. Res. Space Phys.* **2007**, *112*, C11007. [[CrossRef](#)]
8. Larkin, N.K.; Harrison, D.E. Global seasonal temperature and precipitation anomalies during El Niño autumn and winter. *Geophys. Res. Lett.* **2005**, *32*, L16705. [[CrossRef](#)]
9. Yu, J.; Kao, H. Decadal changes of ENSO persistence barrier in SST and ocean heat content indices: 1958–2001. *J. Geophys. Res. Atmos.* **2007**, *112*, D13106. [[CrossRef](#)]
10. Song, W.; Dong, Q.; Xue, C. A classified El Niño index using AVHRR remote-sensing SST data. *Int. J. Remote Sens.* **2016**, *37*, 403–417. [[CrossRef](#)]

11. Ding, R.; Tseng, Y.; Li, J.; Sun, C.; Xie, F.; Hou, Z. Relative Contributions of North and South Pacific Sea Surface Temperature Anomalies to ENSO. *J. Geophys. Res. Atmos.* **2019**, *124*, 6222–6237. [[CrossRef](#)]
12. Xue, C.; Wu, C.; Liu, J.; Su, F. A Novel Process-Oriented Graph Storage for Dynamic Geographic Phenomena. *ISPRS Int. J. Geo-Inf.* **2019**, *8*, 100. [[CrossRef](#)]
13. Liu, J.Y.; Xue, C.J.; Dong, Q.; Wu, C.B.; Xu, Y.F. A Process-Oriented Spatiotemporal Clustering Method for Complex Trajectories of Dynamic Geographic Phenomena. *IEEE Access* **2019**, *7*, 155951–155964. [[CrossRef](#)]
14. Yang, J.; Gong, P.; Fu, R.; Zhang, M.; Chen, J.; Liang, S.; Xu, B.; Shi, J.; Dickinson, R. Erratum: The role of satellite remote sensing in climate change studies. *Nat. Clim. Chang.* **2014**, *3*, 875–883. [[CrossRef](#)]
15. Luo, W.; Yu, Z.-Y.; Xiao, S.-J.; Zhu, A.-X.; Yuan, L.-W. Exploratory Method for Spatio-Temporal Feature Extraction and Clustering: An Integrated Multi-Scale Framework. *ISPRS Int. J. Geo-Inf.* **2015**, *4*, 1870–1893. [[CrossRef](#)]
16. Steinbach, M.; Tan, P.; Boriah, S.; Kumar, V.; Klooster, S.; Potter, C. The application of clustering to earth science data: Progress and challenges. In Proceedings of the 2nd NASA Data Mining Workshop: Issues and Applications in Earth Science Data, Pasadena, CA, USA, 23–24 May 2006; pp. 1–6.
17. Birant, D.; Kut, A. ST-DBSCAN: An algorithm for clustering spatial–temporal data. *Data Knowl. Eng.* **2007**, *60*, 208–221. [[CrossRef](#)]
18. Kawale, J.; Liess, S.; Kumar, A.; Steinbach, M.; Ganguly, A.; Samatova, N.F. Data guided discovery of dynamic climate dipoles. In Proceedings of the NASA Conference on Intelligent Data Understanding, Mountain View, CA, USA, 19–21 October 2011; pp. 30–44.
19. Xue, C.; Dong, Q.; Qin, L. A cluster-based method for marine sensitive object extraction and representation. *J. Ocean Univ. China* **2015**, *14*, 612–620. [[CrossRef](#)]
20. Liu, J.; Xue, C.; He, Y.; Dong, Q.; Kong, F.; Hong, Y. Dual-constraint Spatiotemporal Clustering Approach for Exploring Marine Anomaly Patterns using Remote Sensing Products. *IEEE J. STARS* **2018**, *11*, 3963–3976. [[CrossRef](#)]
21. Long, J.A.; Weibel, R.; Dodge, S.; Laube, P. Moving ahead with computational movement analysis. *Int. J. Geogr. Inf. Sci.* **2018**, *32*, 1275–1281. [[CrossRef](#)]
22. Dodge, S.; Gao, S.; Tomko, M.; Weibel, R. Progress in computational movement analysis—Towards movement data science. *Int. J. Geogr. Inf. Sci.* **2020**, *34*, 2395–2400. [[CrossRef](#)]
23. Mondo, G.D.; Stell, J.G.; Claramunt, C.; Thibaud, R. A graph model for spatio-temporal evolution. *J. Univers. Comput. Sci.* **2010**, *16*, 1452–1477.
24. Del Mondo, G.; Rodríguez, M.; Claramunt, C.; Bravo, L.; Thibaud, R. Modeling consistency of spatio-temporal graphs. *Data Knowl. Eng.* **2013**, *84*, 59–80. [[CrossRef](#)]
25. Liu, W.; Li, X.; Rahn, D. Storm event representation and analysis based on a directed spatiotemporal graph model. *Int. J. Geogr. Inf. Sci.* **2016**, *30*, 1–22. [[CrossRef](#)]
26. Zhu, R.; Guilbert, E.; Wong, M.S. Object-oriented tracking of the dynamic behavior of urban heat islands. *Int. J. Geogr. Inf. Sci.* **2017**, *31*, 405–424. [[CrossRef](#)]
27. Dixon, M.; Wiener, G. TITAN: Thunderstorm identification, tracking, analysis, and nowcasting—A radar-based methodology. *J. Atmos. Ocean. Technol.* **1993**, *10*, 785–797. [[CrossRef](#)]
28. Muñoz, C.; Wang, L.P.; Willems, P. Enhanced object-based tracking algorithm for convective rainstorms and cells. *Atmos. Res.* **2018**, *201*, 144–158. [[CrossRef](#)]
29. Guttler, F.; Ienco, D.; Nin, J.; Teisseire, M.; Poncelet, P. A graph-based approach to detect spatiotemporal dynamics in satellite image time series. *ISPRS J. Photogramm. Remote Sens.* **2017**, *130*, 92–107. [[CrossRef](#)]
30. Xue, C.; Dong, Q.; Xie, J. Marine spatio-temporal process semantics and its applications-taking the El Niño Southern Oscillation process and Chinese rainfall anomaly as an example. *Acta Oceanol. Sin.* **2012**, *31*, 16–24. [[CrossRef](#)]
31. Xue, C.; Liu, J.; Yang, G.; Wu, C. A Process-Oriented Method for Tracking Rainstorms with a Time-Series of Raster Datasets. *Appl. Sci.* **2019**, *9*, 2468. [[CrossRef](#)]
32. Shen, Z.Q.; Wan, R.C. A new approach for converting raster to vector—Node searching. *J. Image and Graph.* **1998**, *3*, 318–321.
33. Robinson, I.; Webber, J.; Eifrem, E. *Graph Database*, 2nd ed.; O'Reilly Media, Inc.: Sebastopol, CA, USA, 2015.
34. Zhang, P.S.; Steinbach, M.; Kumar, V.; Shekhar, S.; Tan, P. Discovery of patterns of Earth science data using data mining. In *Next Generation of Data Mining Applications*; Wiley: Piscataway, NJ, USA, 2005; pp. 167–188.
35. Yan, H.; Sun, G.L.; Liu, X.D. Relationship between ENSO events and regional climate anomalies around the Xisha Islands during the last 50 years. *J. Top. Oceanogr.* **2010**, *29*, 29–35.
36. Wiedermann, M.; Radebach, A.; Donges, J.F.; Kurths, J.; Donner, R.V. A climate network-based index to discriminate different types of El Niño and La Niña. *Geophys. Res. Lett.* **2016**, *43*, 7176–7185. [[CrossRef](#)]
37. Zhang, Z.; Ren, B.; Zheng, J. A unified complex index to characterize two types of ENSO simultaneously. *Sci. Rep.* **2019**, *9*, 8373. [[CrossRef](#)]
38. Kao, H.Y.; Yu, J.Y. Contrasting Eastern-Pacific and Central-Pacific Types of ENSO. *J. Clim.* **2009**, *22*, 615–632. [[CrossRef](#)]
39. Kug, J.S.; Jin, F.F.; An, S.I. Two Types of El Niño Events: Cold Tongue El Niño and Warm Pool El Niño. *J. Clim.* **2009**, *22*, 1499–1515. [[CrossRef](#)]